Study on mechanism of two-phase flow in porous media using X-ray CT Image Analysis

Etude sur le mécanisme de transfert biphasé dans les milieux poreux par l'imagerie aux rayons X

Mukunoki T.
Graduate School of Science and Technology, Kumamoto University, Japan

Mikami K.
Japan Oil Gas and Metal National Corporation, Japan

ABSTRACT: The objective of this study is to understand the mechanism of light non-aqueous phase liquid (LNAPL) migration in sandy soil. This paper introduces a newly developed test apparatus for measuring flow injection of micro-focused X-ray computed tomography (MXCT) scanners, and an image analysis technique. The pore scale and its distribution in the specimen are then evaluated. Only those pore structures trapping LNAPL are extracted, and cluster analysis is applied to each. This image processing technique allows quantitative evaluation of pore scale and pore structures trapping LNAPL.

RÉSUMÉ: L'objectif de cette étude est de comprendre le mécanisme de migration du LNAPL dans un sol sablonneux. Dans cet article, la technique récemment mise au point d'analyse de scanner et d'images par appareil de test d'injection de flux micro-focalisé de tomographie par rayons-X assisté par ordinateur est décrite. L'objectif est d'évaluer l'échelle de porosité et sa répartition dans l'échantillon. Seules les structures poreuses formant les LNAPL sont extraites et une 'analyse de cluster est appliquée à chaque structure poreuse. Cette technique de traitement par image a permis une évaluation quantitative de l'échelle et de la structure poreuse du LNAPL.

KEYWORDS: Multipfase flow, ground contamination, Image Analysis, X-ray CT

1 INTRODUCTION

Multiphase flow is an issue in the study of ground contamination by light non-aqueous phase liquids (LNAPLs), where quantitative parameters regarding particle shape and pore structure are often desired. The basic mechanics of LNAPL migration were developed along with the theory of unsaturated flow mechanics. In recent studies, van Genuchten and Mualem models have been used to deduce the relative permeability coefficient of NAPLs in porous media (Mualem, 1976; van Genuchten, 1980), allowing visualization of the degree of saturation distribution for LNAPLs by numeric simulation (e.g., EPA, 1997). However, LNAPLs flow though pore structures, potentially polluting groundwater due to residual LNAPLs in pores. Characteristics of the pore structure of sand, such as pore size, shape, spatial distribution, and connectivity, are therefore important, and should be evaluated in three dimensions to understand the mechanism of LNAPL capture. Recent technologies such as X-ray computed tomography (CT) scanners have made possible nondestructive evaluation of pore diameter and distribution in the study of fluid behavior in sandy soil (Wildenschild et al., 2002; Altman, 2005; Wildenschild et al., 2005; Al-Kharusi & Blunt, 2007; Mukunoki et al., 2010). New techniques for image processing and analysis of X-ray CT images are thus now required (Mukunoki et al., 2011).

The objective of this study is to understand the mechanism of LNAPL migration in sandy soil. This paper introduces a newly developed test apparatus for injecting fluid for micro-focused X-ray computed tomography (MXCT) scanners, and an image analyzing technique proposed by the authors for evaluating pore scale and distribution. Pore structures trapping LNAPLs are then visualized by cluster analysis, allowing static evaluation of pore scale and structure. Specifications of the micro-focused X-ray CT scanner used in this study are in Mukunoki et al., (2011).

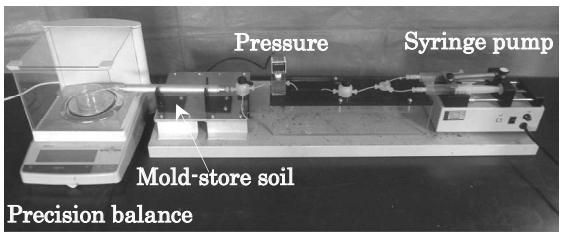

(a) Photograph of test apparatus

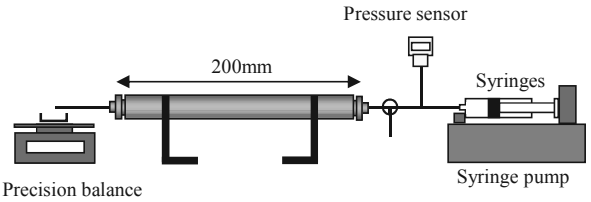

(b) Schematic of test apparatus

Figure 1. MXCT fluid injection test system

1 EXPERIMENTAL METHODS

Figure 1 shows the developed fluid injection test apparatus. An aluminum mold holds the sand sample to be scanned. The inner diameter of this mold is only 10 mm, making gravity effects negligible. Fluids are injected using two syringe pumps with a minimum constant flow velocity of 0.1 cm^3/h. The developed experiment consists of injecting fluids into a 14.61 cm^3 sample. Mass outflow is measured using a precision balance, and the injection rate is controlled through syringes and a syringe pump that allow slow rates. Table 1 shows specifications of the fluids tested. To allow discrimination of LNAPL and water phases using micro CT, iodine potassium was added to the water. This KI water has a density of 1.25 g/cm^3, but its kinematic viscosity is almost the same as that of pure water. The LNAPL used is

Table 1. Specification of fluids tested

Property	LNAPL	KI solution
density ρ (g/cm^3)	0.7486	1.24786
viscosity ν (cP)	1.29	0.9664
Surface tension γ (dyn/cm)	20.0	72.3
contact angle • (degree)	6.4	62.1
interfacial tension γ_{nw}(dyn/cm)	54.5	

Figure 2. A photograph of scene before CT scanning

Table 2. Scan conditions

Voltage (kV)	180
Current (μA)	200
Number of view angles	1500
Projection average	10
Resolution (μm)	5

isoparaffin, which has a fluid density of 0.75 g/cm^3. Figure 2 shows the MXCT experimental setup, and Table 2 shows the scanning conditions.

2 IMAGE PROCESSING ANALYSIS

2.1 *Marker-controlled watershed processing*

X-ray CT images are composed of voxels, called CT-values, which are proportional to the material density. To separate pore space and soil particles in the image, it is necessary to define a threshold value for the CT values. Figure 3 shows an X-ray CT image of Toyoura sand that includes KI solution and LNAPL. That image also includes magnetic sand, so four kinds of CT-value exist in the CT image of Figure 3(a): soil particles, solid-phase magnetic sand particles, KI solution, and liquid-phase LNAPL. Knowing the number of materials in the CT images allows fixing areas of magnetic sand particles, soil particles, LNAPL, and pore space, as well as identifying mixels where two or more materials occupied a single voxel. Watershed processing, which is based on CT-value gradient changes between materials, was applied only to mixel areas in what is called the marker-controlled watershed (MCW) method. Figures 3(b)–(d) show the MCW process. Figure 3(b) is the CT-value profile obtained from lines in the CT image in Figure 3(a). Clarification of the materials in the CT image allows defining the CT-value range for each material without knowing CT-values for the mixel. To evaluate the gradient in the mixel areas, Figure 3(c) shows a profile of the gradient obtained from Figure 3(b). Finally, the coordinate in the CT image with maximum gradient was defined between different materials, and watershed processing was applied to the CT image. This CT-value thresholding technique does not lose spatial geometry information, and is an objective approach for distinguishing the CT threshold values.

2.2 *Image analysis technique for connectivity of pore structure based on mathematical morphology*

Mukunoki et al. (2011) proposed an image processing technique that uses mathematical morphology (Soille, 2002) to evaluate the 3-D distribution of pore scale in dry, sandy soil (a two-phase soil particle and air mixture). We used this method to evaluate

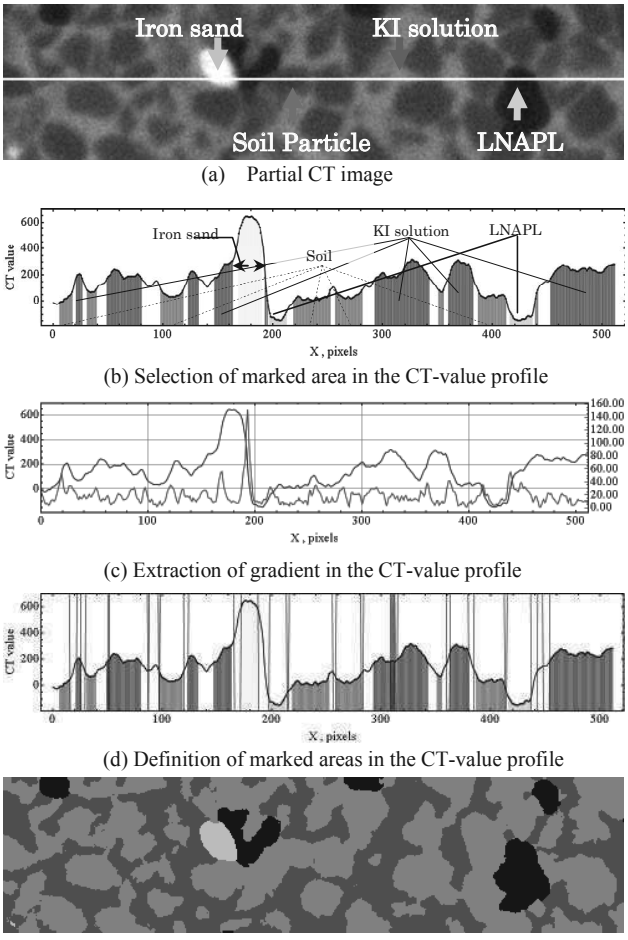

Figure 3. Marker-controlled watershed processing

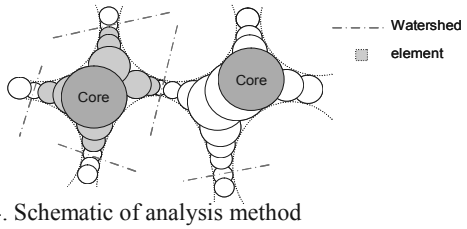

Figure 4. Schematic of analysis method

the volume and diameter of pore water, and showed that LNAPL existed in pore structures. Moreover, connectivity of the pore structure affects flow behavior, and so should be considered in this study. If continuous structures could be isolated as part of a pore structure, a cluster labeling method would give the number of isolated LNAPL blobs and their connectivity. The authors applied the evaluation method of the 3D distribution of pore scale, and used this method to find a circle with minimum diameter as shown in Figure 4. This method successfully separated entire pore structures, making it possible to evaluate spatial distribution of the LNAPL volume.

3 RESULTS AND DISCUSSION

3.1 *LNAPL injection to the sand with saturation of 100%*

Intrinsic permeability (k) of the tested sand was 1.75×10^{-11} m^2 for Case 1 and 1.57×10^{-11} m^2 for Case 2, as obtained from the injection test. In this study, the injection speed was a parameter for this test. Figure 5 shows the difference between inlet and outlet pressures, and the mass of fluid collected at the outlet for Case 1. The injection pore volume (PV) at the break-through

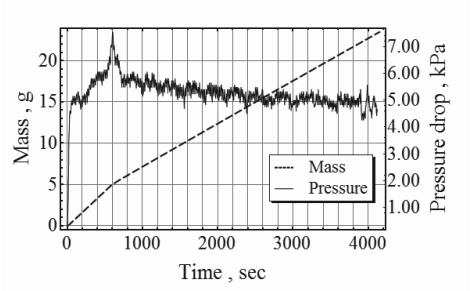

Figure 5. Pressure difference between inlet and outlet and cumulative fluid mass in Case 1

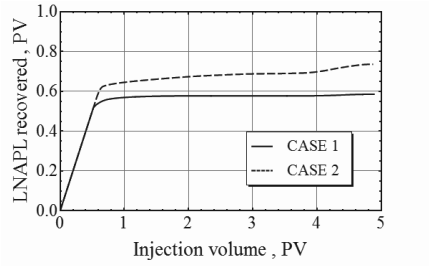

Figure 6. Volume profile of LNAPL recovered in Cases 1 and Case 2

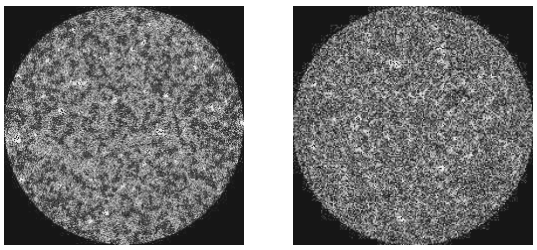

(a) *LNAPL injection* under KI saturation conditions (b) *KI solution* injection after the status of Fig. 7(a)

Figure 7. MXCT images after injecting LNAPL and KI solution

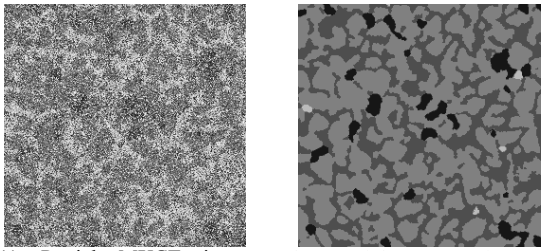

(a) Partial MXCT image before MCW processing (b) Partial MXCT image after MCW processing

Figure 8. MXCT images after MCW processing

point was 0.65 for Case 1 and 0.67 for Case 2. The saturation degree of LNAPL was measured from the injection volume when we observed the LNAPL in the plate at the outlet position. Values were 80.1% for Case 1 and 83.1% for Case 2. These similar values indicate that the prepared samples both had similar pore structures at the initial condition.

3.2 *KI solution injection into sand polluted by LNAPL*

Figure 6 shows the volume profile of LNAPL recovered by KI solution injection. As shown in Figure 6, the injection pore volume at the breakthrough point was 0.51 for Case 1 and 0.56 for Case 2, indicating that the entry pressure for Case 1 was observed earlier than Case 2. To evaluate this phenomenon, the capillary number may help in the following equation (1):

$$Ca = v_w^{dal} \nu_w / \gamma, \quad (1)$$

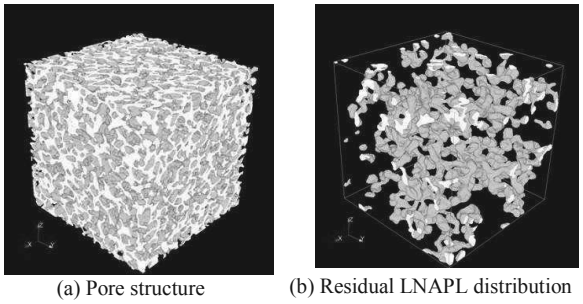

(a) Pore structure (b) Residual LNAPL distribution

Figure 9. MXCT images after MCW processing

where v^{dal} is Darcy's velocity, ν is kinematic viscosity, and γ is the interfacial tension. Subscript w means "wetting." The capillary number *Ca* indicates the ratio of viscosity and interfacial tension , and when *Ca* is less than 10^{-6} multiphase flow should be dominated by capillary pressure (Mayer & Miller, 1993). In other words, a low *Ca* number may cause fingering flow in porous media. In this study, *Ca* for Case 1 was 1.57 x 10^{-6} and *Ca* for Case 2 was 3.14 x 10^{-5}. LNAPL saturation degrees after the KI solution injection test in Case 1 and Case 2 were 21.5% and 9.5%, respectively, confirming that *Ca* greater than 10^{-6} caused less volume of residual LNAPL.

3.3 *Evaluation of pore structure using the MCW method*

Figure 7 shows MXCT images of sand after injecting LNAPL (Figure 7(a)) and KI solution (Figure 7(b)) in Case 1. X-ray CT images are generally 256-level grayscale, with black areas having the least density and white areas the greatest. Figure 7(a) shows that LNAPL was trapped, and its shape was different. Also, the black shape of LNAPL in Figure 7(b) was more circular than as seen in Fig 7(a). These LNAPL blobs are residual LNAPL trapped due to KI solution injecting. Multi-threshold processing with the MCW method was applied to a CT image with 512 × 512 × 512 cubic voxel area. The 4-color MXCT image shown in Figure 8(b) was created from Figure 8(a).

Based on 4-color CT images, only pore structure and residual LNAPL could be extracted from the CT images in Figure 8(b). The porosity obtained from 3D CT images was 40.7% for Case 1 and 38.5% for Case 2. In fact, the porosity calculated from the mean dry density of the sand sample was 39.4%, and the difference should be negligible (<1% error), confirming that multi-threshold processing with MCW gave reasonable values for porosity. Residual LNAPL after injecting the KI solution was 16.7% for Case 1 and 12.6% for Case 2. Measured saturation of residual LNAPL from the mass in the outlet plate was 4.8% less than the obtained value from MCW for Case 1, and 3.1 % greater than that for Case 2.

Figures 9(a) and 9(b) show 3D CT images of pore structure and LNAPL blobs isolated with MCW processing. Pore structure and LNAPL blobs were thus successfully extracted from soil samples in three dimensions without disturbance.

3.4 *Cluster analysis of pore structure*

Figures 10 shows histograms of pore size in Case 1 and Case 2. Frequency in vertical axis means the normalized value by total voxel number of pore structure. Maximum pore size in Case 2 was slightly greater than in Case 1, as shown in Figure 10. There were 1317 pore elements with LNAPL in Case 1 and 1023 in Case 2. Table 3 summarizes saturation degrees of LNAPL for Case1 and Case 2 before and after KI solution injecting obtained from X-ray CT images treating MCW processing. Initially, the sand sample for Case2 had only 3% greater saturation degree of LNAPL than Case 1. However, residual saturation degree of LNAPL for Case 2 was less than

half for Case 1. Figure 11 shows 3D MXCT images of pore structure isolated by mathematical morphology and cluster analysis for Case 1 and Case 2. Cluster analysis of continuous pore structure such as in soil materials allows defining pore elements, allowing for their statistical analysis. In Figure 11, the red cluster with greatest volume has a more complex shape than the blue cluster with small volume, which is shaped like balls. There were 99 LNAPL clusters isolated in Case 1 and 156 in Case 2, implying that fingering flow with capillary force caused by LNAPL remained in wide area in the sample for Case 1. On the other hand, Case 2 with the capillary number (*Ca*) twenty times greater than Case 1 reduced the capillary pressure more than Case 1 as Mayer & Miller, (1993) discussed; and hence, it can be concluded that the fingering flow with capillary force was restrained.

3.5 *Factor of LNAPL trapping*

If LNAPL migrated in a single direction, water should be almost completely flushed out. However, pore structure was distributed in three dimensions, so pore structure connectivity and a three-dimensional bottleneck effect should be considered to evaluate residual LNAPL in the soil. In the case of sandy soil, small changes in capillary pressure in excess of the entry pressure significantly increased or decreased saturation. Factors for trapping LNAPL are thus related to the connectivity of pore structures and drastic changes in capillary pressure with bottleneck effect. Besides, *Ca* would be related to the trapping distribution in the sand as shown in Fig. 11 (a) and (b).

4 CONCLUSIONS

Sandy soil specimens were scanned by micro-focused X-ray CT scanners, and spatial distribution of pore structures with LNAPL were visualized and quantitatively evaluated by a newly developed image processing technique using marker-controlled watershed, a mathematical morphological method, and cluster analysis. Key conclusions are as follows:

1) The developed thresholding technique worked well, and allowed objective definition of locations with changing greatest CT values without histogram analysis.
2) Factors for trapping LNAPL are related to the connectivity of pore structures and drastic changes in capillary pressure with bottleneck effect.
3) The capillary number (*Ca*) more than 10^{-5} reduced the capillary effect and residual LNAPL would be distributed in local position. Meanwhile, the less *Ca* had dominant flow with capillary effect so LNAPL was trapped in wide area of sample.

5 ACKNOWLEDGEMENTS

This research was financially supported by a Grant-in-Aid for Scientific Research (A) No. 23246156, for which Prof. Y. Obara of Kumamoto University is a corresponding researcher. The authors thank Mr. T. Sato of the Faculty of Engineering, Kumamoto University, for his valuable support.

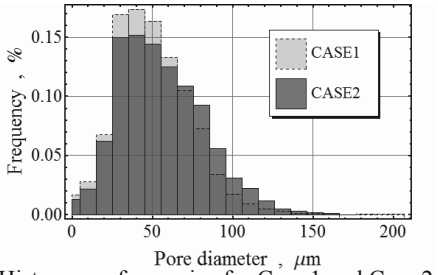

*Fig*ure 10. Histogram of pore size for Case 1 and Case 2

Table 3. Test results

Property	Case 1	Case 2
Initial LNAPL saturation (%)	80.08	83.14
Residual LNAPL saturation (%)	21.48	9.47
Cumulative pore volume at break through	0.51	0.56

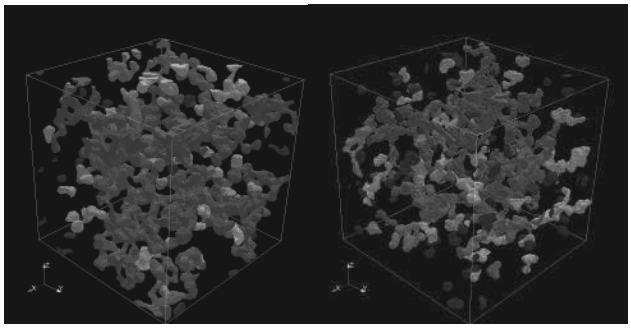

(a) Pore with LNAPL in Case 1 (b) Pore with LNAPL in Case 2

Figure 11. 3D MXCT images of isolated pore structures

6 REFERENCES

Alkharusi, A. and Blunt, M.J. (2007): Network extraction from sandstone and carbonate pore space images, Journal of Petroleum Science and Engineering, Vol.56(4), pp. 219-231.

Altman, J. S., Peplinski, J. W. and Rivers, L. M. (2005), "Evaluation of synchrotron X-ray computerized micro tomography for the visualization of transport processes in low-porosity materials"Journal of Contaminant Hydrology 78, 167– 183.

Dullien F.A.L. (1992), "Porous Media Fluid Transport and Pore Structure", ACADEMIC PRESS.INC. pp132-138.

EPA/600/R-97/102 Environmental Protection Research Laboratory October (1997) Agency Ada, OK 74820 vvEPA NAPL: Simulator Documentation.

Mayer, A.S. and Miller, C.T., : An Experimental Investigation of Pore-Scale Distributions of Nonaqueous Phase Liquids at Residual Saturation, Transport in Porous Media, Vol.10, 57-80, 1993.

Mualem, Y. (1976) : A new model for predicting the hydraulic conductivity of unsaturated porous media. Water Resour. Res., 12:512-522.

Mukunoki, T., Sugimura, K. and Mikami, M. (2010), Visualization of LNAPL contamination in sandy soil using X-ray CT scanner, Proc. of International Symposium on Earth Science and Technology 2010, pp.153-158.

Mukunoki, T., Mikami, K. and Sato, T. (2011), Image simulation of wetting and drying process in sandy soils by μ-focus X-ray CT scanner, Proc. of the 2nd Japan-Korea Joint Workshop on Unsaturated Soils and Ground, pp. 221-228.

Soille, P. : Moephological Image Analysis: Principles and Applications, Springer-Vellag Berlin Heidelberg New York, 2002.

van Genuchten,M.Th (1980) : A closed-form equation for predicting the hydraulic conductivity of unsaturated soil, Soil Sci.Soc.Am.J., Vol144, pp.892-898.

Wildenschild, D., Hopmans, J.W., Vaz, C., Rivers, M.L.,Rikard, D., Christensen, B.S. (2002), "Using X-ray computed micro tomography in hydrology: systems, resolution and limitations", J. Hydrol. 267, 285–297.

Wildenschild, D., Hopmans, J.W., Rivers, M.L., Kent, A.J. (2005), "Quantitative analysis of flow processes in a sand using synchrotron-based X-ray microtomography", Vadose Zone J. 4, 112–126.